Photoacoustics 33 (2023) 100549

Contents lists available at ScienceDirect

Photoacoustics

journal homepage: www.elsevier.com/locate/pacs

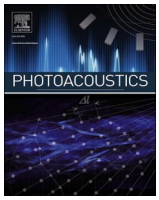

Transfontanelle photoacoustic imaging of intraventricular brain hemorrhages in live sheep

ARTICLE INFO

Keywords
Transfontanelle
Photoacoustic imaging
Neonates
PVH
IVH
Periventricular hemorrhage
Intraventricular hemorrhage

ABSTRACT

Intraventricular (IVH) and periventricular (PVH) hemorrhages in preterm neonates are common because the periventricular blood vessels are still developing up to 36 weeks and are fragile. Currently, transfontanelle ultrasound (US) imaging is utilized for screening for IVH and PVH, largely through the anterior fontanelle. However for mild hemorrhages, inconclusive diagnoses are common, leading to failure to detect IVH/PVH or, when other clinical symptoms are present, use of second stage neuroimaging modalities requiring transport of vulnerable patients. Yet even mild IVH/PVH increases the risk of moderate-severe neurodevelopmental impairment. Here, we demonstrate the capability of transfontanelle photoacoustic imaging (TFPAI) to detect IVH and PVH in-vivo in a large animal model. TFPAI was able to detect IVH/PVH as small as 0.3 mL in volume in the brain ($p < 0.05$). By contrast, US was able to detect hemorrhages as small as 0.5 mL. These preliminary results suggest TFPAI could be translated into a portable bedside imaging probe for improved diagnosis of clinically relevant brain hemorrhages in neonates.

1. Introduction

Intraventricular hemorrhage (IVH) and periventricular hemorrhage (PVH), jointly known as periventricular-intraventricular hemorrhage (PIVH), are common complications in preterm neonates. IVH applies to hemorrhages within the brain's ventricular system, and PVH applies to hemorrhages in the periventricular region [1] (see Fig. 1). PIVH has an incidence rate of 15–25% in low birth weight infants (< 1500 g) and 45–50% in extremely low birth weight infants (< 1000 g) [2,3]. US imaging through fontanelles, which can be described as cranial or transfontanelle US, is the current standard of care diagnostic modality to detect brain hemorrhages [4]. US has demonstrated sensitivity near 100% and specificity near 93% for brain bleeds > 5% but low sensitivity and even lower specificity (i.e., 0–5%) for brain bleeds of < 5% (without obvious blood clots) [5,6]. Moreover, US has very poor sensitivity for detecting small cerebellar hemorrhages (PVH) [6]. Yet smaller hemorrhages and brain bleeds can lead to moderate-severe neurodevelopmental impairment [7] including development of post-hemorrhagic hydrocephalus (PHH) [8]. Treatment of PHH requires neurosurgical interventions for the purpose of placement of a shunt [9]. There is growing evidence that early neurosurgical interventions improve the neurodevelopmental outcome of infants with PHH [10]. A second-stage diagnostic tool, magnetic resonance imaging (MRI) [11], has high sensitivity and specificity for detecting brain hemorrhages but is only prescribed when the neonate exhibits clinical symptoms of neurological damage. Moreover, in most cases MRI requires transporting clinically unstable newborns out of the Neonatal Intensive Care Unit (NICU) for up to an hour or more [12,13], may necessitate anesthesia or sedation that can be associated with risks (i.e. hypotension, hemodynamic changes, or allergic reaction [14]), and has a relatively high cost. Therefore, development of novel non-invasive imaging methods for the detection of low-grade IVH and PVH could have a significant clinical impact by facilitating early neurosurgical and therapeutic interventions for the prevention and treatment of PHH in neonates [15]. Near-infrared spectroscopy (NIRS) is a recent optical imaging modality that can potentially assist clinicians in assessing cerebral perfusion and oxygenation which may indicate IVH [16–18], but has poor spatial resolution and poor penetration depth [19].

Photoacoustic (PA) imaging is a promising technique that provides non-invasive detection of structural, functional, and molecular anomalies in biological tissue [20,21]. It combines the technological advances of both optical and acoustic imaging, i.e., the high intrinsic contrast of optical imaging and the spatial resolution of US imaging [22]. In PA imaging, nanosecond laser pulses illuminate the tissue at the wavelengths of endogenous chromophores such as oxy-hemoglobin (HbO_2) and deoxy-hemoglobin (HbR) [23,24]. The temporary change in temperature caused by the absorption of photons by the chromophores results in a thermal expansion, creating a localized change in pressure. An ultrasonic transducer is used to detect these pressure changes, which manifest as acoustic waves.

In this proof-of-principle study, we assessed the feasibility of transfontanelle PA imaging (TFPAI) for the detection of low grade IVH and PVH, as modeled in live sheep with a surgically created acoustic window in the skull imitating a neonatal fontanelle.

2. Materials and methods

This study was approved by the Office of Animal Care and Institutional Biosafety and the Institutional Animal Care and Use Committee at the University of Illinois at Chicago.

2.1. IVH and PVH model in sheep

The rationale for using a sheep model was the similarity of gyroencephalic morphology and volume between a human preterm neonate and adult sheep brain, the distance to region of interest, e.g.,

https://doi.org/10.1016/j.pacs.2023.100549
Received 28 February 2023; Received in revised form 22 August 2023; Accepted 23 August 2023
Available online 24 August 2023

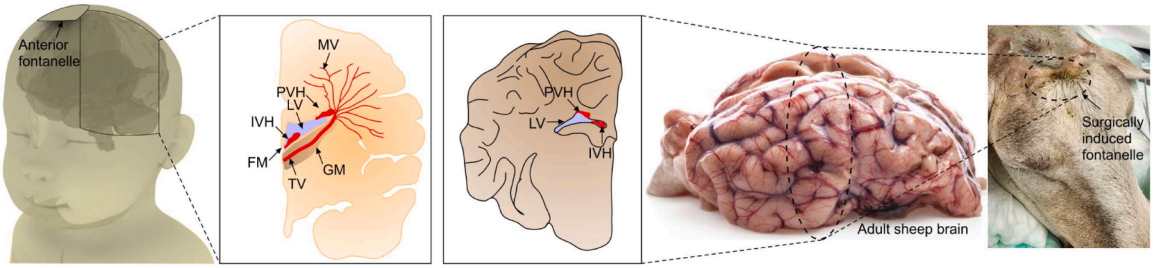

Fig. 1. Demonstration of intraventricular and periventricular hemorrhages in human (left) and sheep (right) brains. Location of constructed fontanelle in sheep head (far right). IVH: intraventricular hemorrhage; PVH: periventricular hemorrhage; MV: medullary veins; FM: foramen of monro; TV: terminal veins; GM: germinal matrix; LV: lateral ventricles.

ventricles from anterior skull location, and its amenability to surgical access through the frontal and parietal skull bones [25–27] (see Fig. 1). While there are animals other than humans that have fontanelles (including dogs and cats), sheep do not have fontanelles at any stage of their life. Rather, the sutures form hard skulls before birth. We mimicked the neonate fontanelle with a 2.5 diameter cranial window (neonate fontanelles range from 0.6 to 3.6 cm [28,29]). For location, the surgery was performed on the anterior of the skull, similar to the location of the anterior fontanelle. Two sheep were used in this study (breed: mix-Katahdin x Dorper, sex: female, weight: 50 kg). We performed a fronto-parietal craniotomy covered by a skin flap to generate a cranial acoustic window that would mimic a fontanelle. The process of creating a cranial acoustic window can be found in [30]. Significant steps were undertaken both during and after surgery to ensure lack of scar tissue or infections that might otherwise compromise the health of the sheep brain. The process of inducing a hemorrhage and the imaging sessions took place long after the craniotomy, when the animal was healed (approx. 3 weeks).

The experimental setup is shown in Fig. 2a and the imaging protocol is shown in Fig. 2f. We injected a heparinized arterial blood sample precisely into the left lateral ventricular space while keeping the right lateral ventricle intact. An autologous arterial blood sample (10 mL) was obtained via an 18 G catheter and transferred into a heparinized (250 IU) syringe. The trajectory of needle insertion was designed so that the needle would travel the shortest distance that avoided sulci or the frontal sinus, or major vessels (Fig. 2c). An infant spinal needle (attached to a Hamilton syringe and connected to an infusion pump) was carefully inserted into the skin along the designed trajectory (guided by real-time

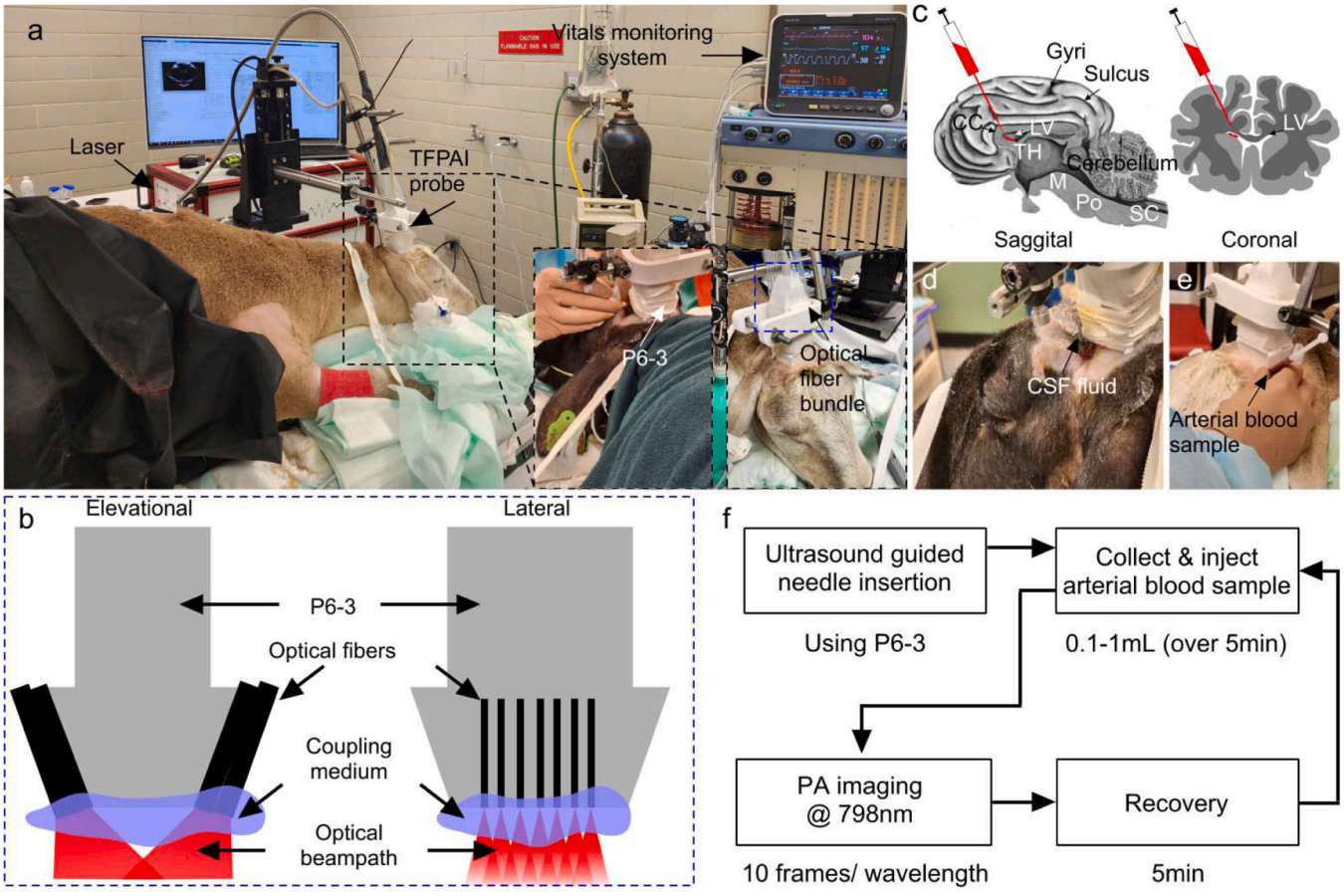

Fig. 2. *In-vivo* experimental setup and imaging protocol. (a) Imaging setup and major components, (b) schematic of TFPAI probe components and optical fiber configuration, (c) schematic of sheep brain sagittal and coronal view demonstrating the location of the blood sample injection pathway to induce hemorrhage, (d) confirmation of needle insertion into a ventricle through release of CSF, (e) photograph of injection of arterial blood sample, and (f) overall imaging protocol. CC: corpus callosum; LV: lateral ventricles; SC: spinal cord; Po: pons; M: Medulla; TH: thalamus; CSF: cerebrospinal fluid.

US imaging), passing through the dura until the planned ventricle location was reached. Confirmation that the needle was positioned correctly (inside the ventricle) was demonstrated by allowing several drops of CSF to flow out of the needle opening (Fig. 2d). Initially, to model the IVH with a low concentration of blood, we injected a small volume of blood (0.1 mL) into the ventricular CSF (Fig. 2e). Simultaneously, we performed the PA imaging session. Subsequently, the volume of blood injected into the ventricle was increased from 0.1 mL to 1.0 mL with a step size of 0.1 mL. To model the low grade PVH, the blood injections were made into the periventricular brain parenchyma using repeating injections of 0.1 mL through the same needle without altering its position. To create both hemorrhage models, a small percentage of the total volume of the sheep brain (~ 250 mL) is used. For both IVH and PVH experiments, we provided a 5 min recovery window between injections.

2.2. TFPAI instrumentation

For the imaging sessions (see Fig. 2a), we used two pulsed Nd:YAG lasers (PhocusMobil, Opotek Inc., CA, USA) with a repetition rate of 10 Hz, pulse width of 7 ns and wavelengths ranging from 690 to 950 nm. A fiber bundle (consisting of 14 fused silica fibers, 1000 μm core diameter, and 220 cm length) with a numerical aperture $NA = 0.22$, (Armadillo SIA (Sunnyvale, CA,USA)), was used for illumination. On the laser side, there were two 10 mm diameter stainless-steel ferrules with active apertures of 4.8 mm, and on the imaging target side, 14 strands of fibers (diameter: 200 μm) (two bunches of 7 fibers each) directed with a 10° angle from the normal axis (see Fig. 2b). Length of fibers was 200 mm. The maximum fluence at the target was limited to 20 mJ/cm^2 to be within ANSI limits [31]. For hemorrhage analysis, we collected images at 798 nm (isosbestic point for oxyhemoglobin and deoxyhemoglobin) [32]. The extinction coefficients for oxyhemoglobin and deoxyhemoglobin in the near infrared region can vary by nearly 10 × depending on the choice of wavelength. Use of an isosbestic point, where the molar extinction coefficients of the two species are the same, reduces sources of error for correlating signal intensity with extent of hemorrhage. For PA signal detection, a P6–3 phased array (Philips Healthcare, TN, USA) US probe with 128-elements (footprint area: 2.04 mm × 0.19 mm) and 4.5 MHz central frequency (−6 dB fractional bandwidth 67.3%, resolution: 0.46 mm) was used [33]. The rationale for using a P6–3 transducer is based on a comparative analysis performed in [33]. Both the optical fiber and the probe position were fixed with clamps and attached to a motorized 3-axis stage for relative positioning and avoiding motion artifacts. PA signal acquisition was performed using a 128-channel, high-frequency, programmable US system (Vantage 128, Verasonics Inc.). For PA image reconstruction we used a filtered back-projection algorithm [34]. Wavelength-dependent fluence compensation was performed following the method described in [35]. We acquired 10 frames at each injected blood sample volume.

2.3. Imaging procedure

At the time of imaging, the animals had intact skin and wool covering the surgically created craniotomy defect (acoustic window). Therefore, before positioning the TFPAI probe, the wool above the cranial window was carefully shaved to expose the skin. A thin layer of US gel was applied to ensure acoustic coupling between TFPAI probe and skin. US B-mode images were utilized as guidance to accurately position the TFPAI probe over the intact skin above the cranial window. Using the US B-mode imaging guidance, the TFPAI probe was placed so that both ventricles can be observed in the cross-section image (Fig. 3a). A photograph of an *ex-vivo* sheep brain (coronal plane), indicating the location of the lateral ventricles, is inset into Fig. 3a for illustrative purposes. Ventricular space (yellow dashed box) is magnified in Fig. 3b. Next, an infant spinal needle was inserted, also guided by simultaneous live US scan. Discharge of CSF through the open needle confirmed needle insertion to the ventricles (Fig. 2d). The needle tip location was observed at the boundary of the left ventricle, as depicted in Fig. 3c.

2.4. Image analysis

We manually specified an IVH or PVH region of interest (ROI) (shown in Fig. 3d-e) for use in analyzing the US and PA reconstructed images. The size of the ROI for IVH analysis was selected based on the fact that it could be located fully within the ventricle (~10 mm^2). The size of the ROI for PVH image analysis was determined by reference to the size of the largest hemorrhage shown in all the PVH reconstructed images (~10 mm^2). ROI_i is the average pixel value within the ROI where the blood was injected (representing detection ability of PA signal associated with an IVH or PVH), and ROI_c is the average pixel value within the ROI on the contralateral side. To obtain results from US images, the same process was repeated.

2.5. Hemorrhage detection

The signal is detectable at a specific volume if it is statistically significantly different than the signal at zero volume (same location, before injection of blood) and more than signal intensity from all lower volume injections. The test is performed by a one-way t-test (signal must be larger than signal at zero volume) with $p < 0.05$. This definition of detectability removes the limitation of an analyst being forced to identify the exact same contralateral region and determine signal strength (and removes the limitation of how to compare slightly asymmetric neonatal ventricles).

3. Results and discussion

We measured the capability of TFPAI to detect IVH and PVH in sheep brain in vivo. A reconstructed US image (coronal plane) shows location of both ventricles relative to the skull base (Fig. 3a) and needle insertion (Fig. 3b and c). Representative PA overlaid US images demonstrating the relative locations of the hemorrhage with respect to the ventricular wall (inside the ventricle ≈IVH and in the subependymal/ periventricular brain parenchyma ≈PVH) are shown.

in Fig. 3d and e, respectively. The analyzed results of US and PA images (mean and range) from two sheep are shown in Figs. 3f and 3g (PVH model) and Fig. 3h and i (IVH model). The amplitudes in Fig. 3f-i are obtained from ROI_i. Results for the contralateral side (ROI_c) as well as the difference between the injected side and contralateral side are presented in Supplementary Fig. 1.

The hemorrhage detection performance of TFPAI was compared to US. In the IVH model, the PA average intensity exhibits a steep pattern of linear growth, Fig. 3i, with increasing injected volumes (i.e., increasing severity of the hemorrhage), even from very low volumes in both sheep. TFPAI was able to detect hemorrhages as small as 0.3 mL in volume in sheep #1 or as small as 0.2 mL in sheep #2. These values correspond to as little as 2–3% bleed in CSF (total cranial blood volume 9–14 mL) [36]. In comparison, the US data (Fig. 3h) showed IVH detection at 0.5 mL in both sheep #1 and #2. US did show reasonable detection and quantification of IVH at higher volumes. In other words, US imaging was able to measure hemorrhagic lesions at ~0.5 mL of blood in the CSF (corresponding to a ~5% bleed), which is in agreement with the results of neonatal clinical studies available in the literature [5,6]. In terms of PVH, TFPAI was able to detect blood volumes as low as 0.2 mL in sheep #1 and 0.3 mL in sheep #2 as shown in Fig. 3g. By comparison, US can detect presence of blood starting at 0.4 mL (sheep #1) or 0.5 mL (sheep #2), Fig. 3f. Above these volumes, US signal does increase monotonically. This study showed that while both US and TFPAI can detect IVH and PVH in our in vivo sheep model, TFPAI has greater sensitivity to detect smaller hemorrhages.

US signal variation may be due to US signal being altered by internal structural reorganization of tissue in response to the presence of

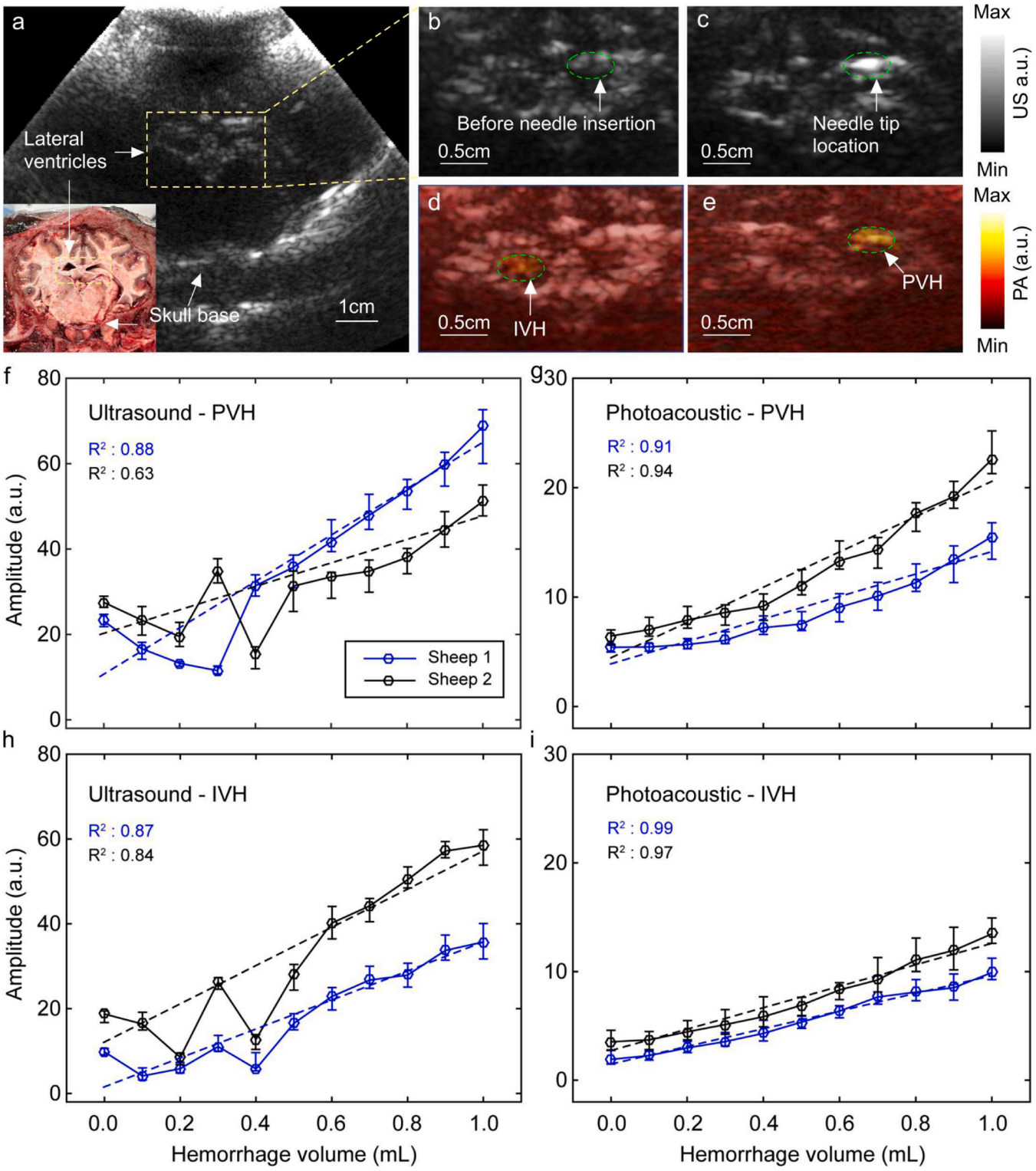

Fig. 3. Capability of TFPAI to detect IVH and PVH. (a) Reconstructed US image (coronal plane) showing lateral ventricle location. A corresponding photograph of the same anatomical cross-section is shown in the inset, (b) lateral ventricles (yellow dashed box in (a)) magnified before needle insertion, (c) lateral ventricles (yellow dashed box in (a)) magnified after needle insertion, (d) reconstructed PA image overlaid on the US image demonstrating IVH within a ventricle, (e) reconstructed PA image overlaid on the US demonstrating PVH just outside the ventricular space, (f-i) averaged pixel values of the injected ROI_i in sheep #1 and #2 shown separately for different injection volumes (mean and range): (f) in the US image to model PVH, (g) in the PA image to model PVH, (h) in the US image to model IVH, (i) in the PA image to model IVH. ROI: region of interest; PA: photoacoustic; US: ultrasound; IVH: intraventricular hemorrhage; PVH: periventricular hemorrhage. As described in the text, the plane of the brain shown in b/c is several mm away from the plane shown in figures d/e in order to illustrate needle placement.

hemorrhage, which is a slight effect, and which would be present whether the hemorrhage is induced or naturally occurring. The effect is not seen in PA, presumably, because PA tracks chromophores (blood) more strongly than other tissue structures.

Although baseline readings did vary between the sheep, in TFPAI for each sheep, the increase in hemorrhage volume corresponded with increased signal for both the IVH and PVH models. The PVH model showed less linearity than IVH at the lowest volumes. This may be because at lower volumes of injected blood, less PA signal is induced at the site of the hemorrhage. Such PA signal travels towards the transducer according to $P_o e^{-\mu a d}$, where P_o is the initial pressure generated, μ_a is the attenuation coefficient (a combination of the effect of acoustic absorption and scattering), and d is the distance traveled through the medium. At lower blood volumes, some of the initial pressure waves die out or become lower than the noise equivalent power (NEP) of the transducer through the random scattering process. With higher volumes of injected blood, the dying out of pressure waves due to random scattering events will be decreased and a more linear change in the correspondence between blood volume and PA signal will be observed. Moreover, for IVH, there is lower scattering within the CSF (inside the ventricle) and therefore the initial pressure waves have more opportunities to merge before they pass through the highly scattering brain tissue. This could explain why a linear signal is observed starting at a lower volume in IVH.

Some limitations of the current study can be addressed in future work. For example, based on our experience, the positioning of the probe on the fabricated sheep fontanelle is very important and sometimes time-consuming (the sheep's head is fully healed at the time of imaging). We expect this can also be a problem when imaging through neonatal fontanelles. Finding the fontanelle and acquiring high quality US images depends on the experience of the US technician [37]. The results could be affected if not enough time is spent on such optimization, both with regards to the location of transducer and light illumination. However, in our experiment, the probe positioning is not altered between collection of US and PA data, so the results would expect to be equally affected in both modalities. In addition, after having collected and analyzed the results of our TFPAI system, it appears to us that a 3-dimensional ROI might be able to better capture the extent of hemorrhage within the brain, which has motivated us to implement a 3D-TFPAI system. Other methods for increasing PA image quality could also be addressed. Quantification might be improved by the use of a different image reconstruction algorithm. Although the PA results include linear compensation for pulse-to-pulse laser fluctuations, non-linear effects, which are a small but nonzero aspect of the PA signal, cannot be compensated for in a straightforward manner and in this analysis, have not been accounted for. This has a small effect on larger PA signals, but could be important for quantification of weak PA signals. Finally, in TFPAI, the detected bandwidth of the received PA signal is limited to those obtained from commercially-available transducers. A wider bandwidth, more sensitive transducer would be expected to generate stronger signals.

4. Conclusions

The results of the current study have demonstrated that TFPAI signal intensity is strongly correlated with the concentration of blood in ventricular CSF and volume of blood in a periventricular lesion. The results indicate that TFPAI potentially outperforms conventional B-mode transfontanelle US, demonstrating lower limits of detection for IVH and PVH. Because both methods utilize the same transducers, the difference in sensitivity may well be related to the physics underlying the two imaging modalities (i.e., acoustic scattering of blood in US imaging versus absorption of blood in PA imaging) [38]. Because it uses the same transducer as US, TFPAI could easily be integrated into the workflow of NICU for highly accurate hemorrhage detection.

Funding

This work was supported by the National Institutes of Health R01EB027769-01, and R01EB028661-01.

CRediT authorship contribution statement

Juliana B. Lara: Data curation, Methodology, Validation. **Rayyan Manwar:** Conceptualization, Data curation, Formal analysis, Methodology, Software, Validation, Writing – original draft, Writing – review & editing. **Laura S McGuire:** Data curation, Methodology. **Md. Tarikul Islam:** Data curation, Software, Writing – original draft. **Seyed Mohsen Ranjbaran:** Conceptualization, Data curation, Formal analysis. **Anthony Shoo:** Writing – review & editing. **Fady T Charbel:** Writing – review & editing. **Martha G. Menchaca:** Writing – review & editing. **Amanda P. Siegel**: Formal analysis, Writing – review & editing. **De-Ann Pillers:** Writing – review & editing. **Juri G. Gelovani:** Conceptualization, clinical needs analysis, clinical applications, animal model optimization, data interpretation, manuscript preparation. **Kamran Avanaki:** Conceptualization, Data curation, Formal analysis, Funding acquisition, Methodology, Project administration, Resources, Software, Supervision, Validation, Writing – original draft, Writing – review & editing.

Declaration of Competing Interest

The authors declare that they have no known competing financial interests or personal relationships that could have appeared to influence the work reported in this paper.

Appendix A. Supporting information

Supplementary data associated with this article can be found in the online version at doi:10.1016/j.pacs.2023.100549.

References

[1] M. Adhikari, E. Gouws, P.K. Desai, Periventricular hemorrhage in a developing world is drug intervention appropriate, Brain Dev. vol. 17 (3) (1995) 164–168, https://doi.org/10.1016/0387-7604(95)00016-5, 1995/05/01.
[2] D. Szpecht, M. Szymankiewicz, I. Nowak, J. Gadzinowski, Intraventricular hemorrhage in neonates born before 32 weeks of gestation—retrospective analysis of risk factors, Child'S. Nerv. Syst. vol. 32 (8) (2016) 1399–1404.
[3] D. Wilson-Costello, H. Friedman, N. Minich, A.A. Fanaroff, M. Hack, Improved survival rates with increased neurodevelopmental disability for extremely low birth weight infants in the 1990s, Pediatrics vol. 115 (4) (2005) 997–1003.
[4] J.J. Volpe, Neurology of the Newborn E-Book, Elsevier Health Sciences, 2008.
[5] S.C. Carson, B.S. Hertzberg, J.D. Bowie, P.C. Burger, Value of sonography in the diagnosis of intracranial hemorrhage and periventricular leukomalacia: a postmortem study of 35 cases, Am. J. Neuroradiol. vol. 11 (4) (1990) 677–683.
[6] J. Intrapiromkul, F. Northington, T.A. Huisman, I. Izbudak, A. Meoded, A. Tekes, Accuracy of head ultrasound for the detection of intracranial hemorrhage in preterm neonates: comparison with brain MRI and susceptibility-weighted imaging, J. Neuroradiol. vol. 40 (2) (2013) 81–88, https://doi.org/10.1016/j.neurad.2012.03.006.
[7] A. Mukerji, V. Shah, P.S. Shah, Periventricular/Intraventricular hemorrhage and neurodevelopmental outcomes: a meta-analysis, Pediatrics vol. 136 (6) (2015) 1132–1143, https://doi.org/10.1542/peds.2015-0944.
[8] Q. Chen, et al., Post-hemorrhagic hydrocephalus: recent advances and new therapeutic insights, J. Neurol. Sci. vol. 375 (2017) 220–230.
[9] E.A. Christian, E.F. Melamed, E. Peck, M.D. Krieger, J.G. McComb, Surgical management of hydrocephalus secondary to intraventricular hemorrhage in the preterm infant, J. Neurosurg.: Pediatr. vol. 17 (3) (2016) 278–284.
[10] V. Garcia-Navarro, et al., Early intervention and neurodevelopmental outcome of infants with posthemorrhagic hydrocephalus: a case series and literature review, Clin. Neurol. Neurosurg. vol. 201 (2021), 106432.
[11] J.J. Volpe, P. Herscovitch, J.M. Perlman, K.L. Kreusser, M.E. Raichle, Positron emmission tomography in the asphyxiated term newborn: parasagittal impairment of cerebral blood flow, Ann. Neurol. vol. 17 (3) (1985) 287–296, https://doi.org/10.1002/ana.410170312.
[12] BWH. Neonatal Intensive Care Unit Parent Information Sheet Brain MRI for my preterm baby. Brigham and Women's Hospital. https://www.brighamandwomens.org/assets/BWH/pediatric-newborn-medicine/pdfs/termeq-mri-parentinfo.pdf (Accessed.

[13] MyHealth.Alberta.ca. MRI of the Head: About your child's test. https://myhealth.alberta.ca/Health/aftercareinformation/pages/conditions.aspx?hwid=abo4435#:~:text=The%20test%20usually%20takes%2030,take%20up%20to%202%20hours (accessed.
[14] R.W. Hall, R.M. Shbarou, Drugs of choice for sedation and analgesia in the NICU, Clin. Perinatol. vol. 36 (1) (2009) 15–26, https://doi.org/10.1016/j.clp.2008.09.007.
[15] R. Manwar, M.T. Islam, A. Shoo, D.A. Pillers, K. Avanaki, Development of Ex-vivo brain hemorrhage phantom for photoacoustic imaging, J. Biophotonics (2023), e202200313.
[16] H.U. Bucher, A.D. Edwards, A.E. Lipp, G. Duc, Comparison between near infrared spectroscopy and 133Xenon clearance for estimation of cerebral blood flow in critically Ill preterm infants, 01/01/online, *Pediatr. Res.*, Regul. Artic. vol. 33 (1993) 56, https://doi.org/10.1203/00006450-199301000-00012.
[17] A.D. Edwards, C. Richardson, M. Cope, J.S. Wyatt, D.T. Delpy, E.O.R. Reynolds, Cotside measurement of cerebral blood flow in Ill newborn infants by near infrared spectroscopy, Lancet vol. 332 (8614) (1988) 770–771, https://doi.org/10.1016/S0140-6736(88)92418-X, 1988/10/01/.
[18] Shankar P. Gopinath, Claudia S. Robertson, Charles F. Contant, Raj K. Narayan, Robert G. Grossman, Britton Chance, Early detection of delayed traumatic intracranial hematomas using near-infrared spectroscopy, J. Neurosurg. vol. 83 (3) (1995) 438–444, https://doi.org/10.3171/jns.1995.83.3.0438.
[19] R.N. Aslin, J. Mehler, Near-infrared Spectroscopy for Functional Studies of Brain Activity in Human Infants: Promise, Prospects, and Challenges, SPIE, 2005, p. 3.
[20] C. Demene, et al., Functional ultrasound imaging of brain activity in human newborns, Sci. Transl. Med. vol. 9 (411) (2017), https://doi.org/10.1126/scitranslmed.aah6756.
[21] R. Manwar, et al., Development and characterization of transfontanelle photoacoustic imaging system for detection of intracranial hemorrhages and measurement of brain oxygenation: Ex-vivo, Photoacoustics (2023), 100538.
[22] B.-F. Osmanski, S. Pezet, A. Ricobaraza, Z. Lenkei, M. Tanter, Functional ultrasound imaging of intrinsic connectivity in the living rat brain with high spatiotemporal resolution, Nat. Commun. vol. 5 (2014) 5023.
[23] L.V. Wang, Tutorial on photoacoustic microscopy and computed tomography, IEEE J. Sel. Top. Quantum Electron. vol. 14 (1) (2008) 171–179.
[24] J.-M. Yang, et al., Simultaneous functional photoacoustic and ultrasonic endoscopy of internal organs in vivo, Nat. Med. vol. 18 (8) (2012) 1297. ⟨https://www.ncbi.nlm.nih.gov/pmc/articles/PMC3885361/pdf/nihms377390.pdf⟩.
[25] C. Mallard, Z.S. Vexler, Modeling ischemia in the immature brain: how translational are animal models, Stroke vol. 46 (10) (2015) 3006–3011.
[26] D.K. Stevenson, W.E. Benitz, P. Sunshine, S.R. Hintz, M.L. Druzin, Fetal and neonatal brain injury, Cambridge University Press,, 2017.
[27] C.E. Williams, A.J. Gunn, C. Mallard, P.D. Gluckman, Outcome after ischemia in the developing sheep brain: an electroencephalographic and histological study, Ann. Neurol. vol. 31 (1) (1992) 14–21.
[28] D.H. Woldeyes, M.D. Kiros, B.A. Abegaz, A.A. Woya, The size of anterior fontanelle and its determinants at birth among neonates in Northern Ethiopia: a cross-sectional study, (in eng), Pediatr. Health Med. Ther. vol. 11 (2020) 477–483, https://doi.org/10.2147/phmt.S283857.
[29] G.A. Popich, D.W. Smith, Fontanels: range of normal size, J. Pediatr. vol. 80 (5) (1972) 749–752.
[30] R. Manwar, et al., Transfontanelle photoacoustic imaging for in-vivo cerebral oxygenation measurement, Sci. Rep. vol. 12 (1) (2022) 1–7.
[31] L. I. o. America, American National Standard for Safe Use of Lasers ANSI Z136. 1–2014, ed: American National Standards Institute, Inc Washington, DC, 2014.
[32] S. Prahl. Optical Absorption of Hemoglobin. https://omlc.org/spectra/hemoglobin/ (accessed.
[33] R. Manwar, M.T. Islam, S.M. Ranjbaran, K. Avanaki, Transfontanelle photoacoustic imaging: ultrasound transducer selection analysis, Biomed. Opt. Express vol. 13 (2) (2022) 676–693.
[34] M. Xu, L.V. Wang, Universal back-projection algorithm for photoacoustic computed tomography, Phys. Rev. E vol. 71 (1) (2005), 016706, https://doi.org/10.1103/PhysRevE.71.016706.
[35] R. Manwar, K. Kratkiewicz, K. Avanaki, Investigation of the effect of the skull in transcranial photoacoustic imaging: a preliminary ex vivo study, Sensors vol. 20 (15) (2020) 4189.
[36] Z. Lu, J. He, Y. Yu, Z. Li, Z. Li, J. Gong, Measurement of lateral ventricle volume of normal infant based on magnetic resonance imaging, Chin. Neurosurg. J. vol. 5 (02) (2019) 65–70.
[37] D. deCampo, M. Hwang, Characterizing the neonatal brain with ultrasound elastography, Pediatr. Neurol. vol. 86 (2018) 19–26, https://doi.org/10.1016/j.pediatrneurol.2018.06.005, 2018/09/01/.
[38] I. Fontaine, M. Bertrand, G. Cloutier, A system-based approach to modeling the ultrasound signal backscattered by red blood cells, Biophys. J. vol. 77 (5) (1999) 2387–2399.

Juliana Benavides-Lara was born in Bogota, Colombia. She received her B.Sc. in Physics in 2017 and her MSc in Physics in 2021 from the National University of Colombia. Currently, she is a research assistant and Ph.D. Student at OPIRA LAB in the Biomedical Engineering Department at the University of Illinois at Chicago, USA. Her research interests include ultrasound and photoacoustic imaging.

Rayyan Manwar received his Ph.D. from University of Windsor, Windsor, Ontario in 2017. His bachelor's was in Electrical and Electronic Engineering from Islamic University of Technology (IUT), Bangladesh in 2011. Currently, he is a research specialist at OPIRA LAB, Biomedical Engineering Department at University of Illinois at Chicago. Previously, he was a post doctoral fellow in Bioengineering Department at Wayne State University, Detroit, MI. His research interests include MEMS based design, fabrication and characterization, photoacoustic and ultrasound imaging.

Laura S McGuire is a Neurosurgery Clinical Instructor and Endovascular/Cerebrovascular Fellow at University of Illinois Chicago.

Md. Tarikul Islam was born in Patuakhali, Bangladesh. He received his B.Sc. in Computer Science and Engineering from Patuakhali Science and Technology University (PSTU) in 2016 and MSc in Electrical and Electronics Engineering from Universiti Kebangsaan Malaysia (UKM), Malaysia. Now he is a research assistant and Ph.D. Student at Biomedical Engineering Department in The University of Illinois at Chicago, USA. His current research interest is on Photoacoustic, Thermoacoustic and Microwave imaging.

Anthony Shoo obtained his medical degree from Howard University College of Medicine in 2012. He then went on to complete his pediatric residency from the University of Nevada School of Medicine in Las Vegas. Following residency, he worked as a general pediatrician for a private practice in Las Vegas, Nevada. In 2020 he attended the University of Illinois at Chicago Medical Center where he is currently a fellow in the field of neonatal-perinatal medicine.

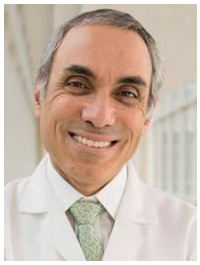

Dr. Fady T Charbel is head of the Department of Neurosurgery at UI (University of Illinois) Health. Dr. Charbel is an internationally recognized clinical expert, researcher, and educator in the areas of stroke; brain aneurysm and cerebrovascular diseases; cerebral blood flow metabolism; and complex cerebral tumors. Dr. Charbel has been named one of America's Top Surgeons by Consumers Research Council of America and listed among America's Top Doctors by Castle Connolly. He has been invited worldwide to lecture, teach, and demonstrate complex surgical procedures. Dr. Charbel is the Dr. Richard L. and Gertrude W. Fruin Professor of Neurosurgery at the University of Illinois College of Medicine.

Dr. Martha G. Menchaca practices in the Department of Radiology at UI Health. Dr. Menchaca specializes in diagnostic radiology, and she certified by the American Board of Radiology.

Amanda P Siegel is a research specialist in bioengineering in collaboration with department of bioengineering, Department of Microbiology, and Immunology, and Department of Biophysics at Rush University.

De-Ann Pillers is the head of the Section of Neonatology at UI Health. In her role, she assures the continued success of clinical neonatology programs and supports the scholarly pursuit of excellence in newborn medicine.

Juri George Gelovani is a world-renown leader in molecular and functional imaging, and the founder of molecular-genetic and epigenetic imaging fields. He started his academic career at the University of Tartu, Estonia in 1989, then he joined Memorial Sloan-Kettering Cancer Center (New York, NY) in 1991 as a Postdoctoral Fellow; in 2003 joined the Univerisy of Texas MD Anderson Cancer Center (Houston, TX) as Full Professor, Deapartment Chair, and Imaging center Director; in 2012 moved to Wayne State University (WSU) and Karmanos Cancer Institute (Detroit, MI) as Department Chair, Imaging Program Leader, and Director of Engineering in Medicine. In 2020, he moved to the United Arab Emirates University, UAEU (Al Ain, UAE).

Kamran Avanaki is currently an Associate Professor of Biomedical Engineering Department at the University of Illinois in Chicago. Prior to this position, he was an Associate Professor of Biomedical Engineering Department at Wayne State University. He received his Ph.D. degree from the University of Kent, the United Kingdom with an Outstanding Achievement Honor in Medical Optical Imaging and Computing in 2012. His areas of expertise are design and development of photoacoustic imaging technology and optical coherence tomography for biomedical applications to solve critical problems in brain and skin imaging.

Juliana Benavides-Lara, Rayyan Manwar
Richard and Loan Hill Department of Bioengineering, University of Illinois at Chicago, Chicago, IL, United States

Laura S. McGuire
Department of Neurological Surgery, University of Illinois at Chicago – College of Medicine, Chicago, IL, United States

Md. Tarikul Islam
Richard and Loan Hill Department of Bioengineering, University of Illinois at Chicago, Chicago, IL, United States

Anthony Shoo
Section of Neonatology, Department of Pediatrics, UIHealth Children's Hospital of the University of Illinois at Chicago, Chicago, IL, United States

Fady T. Charbel
Department of Neurological Surgery, University of Illinois at Chicago – College of Medicine, Chicago, IL, United States

Martha G. Menchaca
Section of Neonatology, Department of Pediatrics, UIHealth Children's Hospital of the University of Illinois at Chicago, Chicago, IL, United States

Amanda P. Siegel
Richard and Loan Hill Department of Bioengineering, University of Illinois at Chicago, Chicago, IL, United States

De-Ann M. Pillers
Section of Neonatology, Department of Pediatrics, UIHealth Children's Hospital of the University of Illinois at Chicago, Chicago, IL, United States

Juri G. Gelovani
Provost Office, College of Medicine and Health Sciences, United Arab Emirates University, Al Ain, Abu Dhabi, UAE
Department of Biomedical Engineering, College of Engineering and School of Medicine, Wayne State University, Detroit, MI 48201, United States
Dept. Radiology, Siriraj Hospital, Mahidol University, Bangkok 10700, Thailand

Kamran Avanaki*
Richard and Loan Hill Department of Bioengineering, University of Illinois at Chicago, Chicago, IL, United States
Section of Neonatology, Department of Pediatrics, UIHealth Children's Hospital of the University of Illinois at Chicago, Chicago, IL, United States
Department of Dermatology, University of Illinois at Chicago, Chicago, IL, United States

* Corresponding author at: Richard and Loan Hill Department of Bioengineering, University of Illinois at Chicago, Chicago, IL, United States.
E-mail address: avanaki@uic.edu (K. Avanaki).